Article

A pH-controlled intelligent inhibitor based on PAM hydrogel for steel corrosion protection in wide range pH NaCl medium

Qing Yang [1], Bing Lin [1*], Junlei Tang [1,2*], Yingying Wang [3], Hongpeng Zheng [1], Hailong Zhang [1,4], Zhen Nie[5], Yanna Zhang [5]

1 School of Chemistry and Chemical Engineering & Institute for Carbon Neutrality, Southwest Petroleum University, Chengdu 610500, China; 1139716217@qq.com (Q.Y); h1900@foxmail.com (B.L); tangjunlei@126.com (J.T); zhp-corrosion@163.com (H.Z); hailong0902@126.com (H.Z).
2 Tianfu Yongxing Laboratory, Chengdu 610217, China.; tangjunlei@126.com (J.T).
3 Key Laboratory of Optoelectronic Chemical Materials and Devices (Ministry of Education), Jianghan University, Wuhan 430056, China. yingyingwanglyon@126.com (Y.W).
4 Research Institute of Tianfu New Energy, Chengdu 610217, China. hailong0902@126.com (H.Z).
5 Research Institute of Petroleum Exploration and Development, CNPC, Beijing 100083, China. niezhen@petro-china.com.cn (Z.N); zhangyanna@petrochina.com.cn (Y.Z)
* Correspondence: tangjunlei@126.com (J.T); h1900@foxmail.com (B.L)

Abstract: To provide carbon steel a long corrosion protection effect in NaCl solution with various pH, a pH-controlled intelligent inhibitor based on poly-acrylamide (PAM) and oleate imidazoline (OIM) was synthesized. SEM, FT-IR and TGA results indicating the OIM inhibitor was successfully loaded into PAM hydrogel with a very high content (39.64 wt%). The OIM release behavior from hydrogel structure have two stages, quickly release and sustained release. The pH of solution could affect the initial release kinetics of OIM inhibitor and the diffusion path in hydrogel structure. Weight loss measurement of L80 steel in different pH solution with OIM@PAM proved the inhibitor responsive release mechanism and anti-corrosion performance. The inhibition efficiency of OIM@PAM can maintain over 80% after long term immersion in harsh corrosive environment (pH 3), which is much higher than the inhibition efficiency of inhibitor in moderate corrosive solution.

Keywords: Intelligent corrosion inhibitor; Oleate imidazoline; Polyacrylamide; pH-controlled release; L80 carbon steel

1. Introduction

Corrosion leads to the material degradation in various environment, which is due to the inter chemical and electrochemical actions between metal substrate and environments[1]. Organic inhibitors have been wildly used to solve the corrosion issue due to their high inhibition efficiency, wild application range, good solubility and relatively low toxicity[2–4]. The inhibition mechanism of organic inhibitor has been explained from the formation of adsorption film. Organic inhibitor adsorbed on metal surface through the delocalized electrical charge on the heteroatoms such as N, S and O[1,5]. Many scholars have focused on the effect of inhibitor functional group type, quantity, and molecular structure on the inhibition efficiency[5]. While, there are several drawbacks to direct use inhibitor in aqueous corrosion environment. To ensure the corrosion protection effect of organic inhibitor, the excessive use of inhibitor will lead to a waste of resources. And the inhomogeneous distribution of inhibitor in corrosive environment will limit the long-lasting effect and anticorrosion effect of inhibitor. In addition, inhibitor is a high selectivity corrosion protection method, which means the inhibitor usually suitable for a certain material and corrosion environment.

Recently, scholars became interested in encapsulating corrosion inhibitor in container to extend the inhibitor protection time and enhance anticorrosion effectiveness as the drawbacks of direct use inhibitor. Many researches try to encapsulate organic inhibitor in to MOFs[6], hollow particles[7], core-shell nanofiber[8], gel materials[9], and so on. One important application of encapsulated inhibitor is to provide self-healing property to

 doi:10.20944/preprints202212.0512.v1

organic coating[6–9]. While the low inhibitor concentration and complex construction of self-healing coating limited the industrial applications. Another important application of encapsulated corrosion inhibitor is intelligent inhibitor. The inhibitor release behavior from encapsulated inhibitor is adjusted according the change of environment by modification the inhibitor container. Wang et al.[10]reported a calcium alginate gel capsules loaded with inhibitor. The synthesized capsules could release inhibitors during the sinking process, and effectively prevent the tube in oil well from corrosion. Dong and his coworkers [11–13] reported a series of intelligent inhibitor. The container could release inhibitor faster in acidic environment in compare with neutral environment, and provide better anticorrosion performance.

Hydrogels material is a hydrophilic 3D natural or synthetic polymer network structural gel, which could swell in water. Hydrogel has been used in drug delivery systems due to the controllable release rate[14]. Researches have tried to use hydrogel in corrosion protection system. Wen et al.[15] reported an intelligent hybrid hydrogel coating for steel corrosion protection. The weight percentage of loaded inhibitor is about 10%, and the releasing property of inhibitor rises as the external environment pH value decrease. Dong et al.[11] have tried to use hydrogel to synthesize intelligent inhibitor, which benefits in long term corrosion inhibition due to the sustained inhibitor supply. Hydrogels is an ideal container material to synthesize intelligent inhibitor, and still need further investigation on increasing the inhibitor content, controlling inhibitor release behavior, and enhance the mechanical property to make the application of intelligent inhibitor based on hydrogel.

Owing to the advantages of excellent corrosion protection performance, low-toxicity, stable and low economy cost, imidazoline and its' derivatives are widely utilized in the industrial fields. The high inhibition efficiency of oleate imidazoline (OIM) derivatives is associated with the good adsorption characteristics and the ability to form a hydrophobic film on metal surface [9,16]. Imidazoline and it's derivatives has excellent inhibition effect in acid [17], neutral [18] and alkaline [19] medium. In our previous work[9], OIM was introduced into gel coating to enhance the anti-corrosion performance of coating in 3.5 wt.% NaCl. In this study, the anti-corrosion performance is mainly dependent on the physical shielding effect of the coating, but the combination of gel material and corrosion inhibitor to enhance the anti-corrosion performance is feasible and effective. Inspired by this work, gel material could be an ideal carrier for encapsulating material to protect the carbon steel. The controllable release behavior of inhibitor could enhance the environment applicability and protection time. Therefore, the drawbacks of directly use inhibitor in aqueous corrosion environment would be significantly improved.

In this work, A pH-controlled intelligent inhibitor based on PAM hydro-gel and OIM were successfully synthesized. SEM, FT-IR, TGA, and mechanical test was employed to investigate the structure and characteristics of OIM@PAM. The OIM release behavior of OIM@PAM in various pH value aqueous environment was studied by UV-visible spectrophotometer, and the release mechanism is discussed in-depth. The outstanding anti-corrosion performance of OIM@PAM in different pH corrosion medium was carried out by weight loss measurement and SEM observation. And the intelligent inhibitor might be applicable for the corrosion protection of facilities and pipelines in oil production.

2. Materials and Methods

2.1 Synthesis of OIM@PAM intelligent corrosion inhibitor

Acrylamide (AM), N,N-methylene-bis-acrylamide (BIS), ammonium persulfate (APS), tetramethylethylenediamine (TEMED) and oleate imidazoline (OIM) all purchased from Shanghai Macklin Biochemical Technology Co., Ltd for the preparation of the intelligent corrosion inhibitor.

Firstly, as Figure1 shown, 1.88 g acrylamide (AM) was dissolved into 5 mL deionized water. Secondly, 1 g oleic imidazoline (OIM) was dispersed to the above solution with continuously stirring until the inhibitor dissolve completely. Followed by adding 0.032 g N,N-methylene-bis-acrylamide (BIS) to the mixed solution, and all of the above steps were processed under the temperature range of 0℃-4℃ to prevent acrylamide from

Preprints (www.preprints.org) | NOT PEER-REVIEWED | Posted: 27 December 2022 doi:10.20944/preprints202212.0512.v1

polymerizing prematurely. Thirdly, 0.015 g ammonium persulfate (APS) was introduced into above solution to convert acrylamide monomers to free radicals. The free radicals would react with unactivated monomers to begin the polymerization chain reaction. While the addition of TEMED was aim to accelerate the rate of formation free radicals from APS and consequently catalyzing polymerization. After that, the as-prepared mixed solution was poured into a silica gel mold (20 mm × 20 mm × 20 mm) and polymerized at 45 ℃ for 12 h. Finally, after drying in vacuum oven (D2T-6050, Jinghong Experimental Equipment Co., Ltd., Shanghai) at 45 °C for 24 h, the intelligent corrosion inhibitor was successfully synthesized and recorded as OIM@PAM. The average weight of obtained OIM@PAM is 2.5583 g and the side length is 12.5 mm.

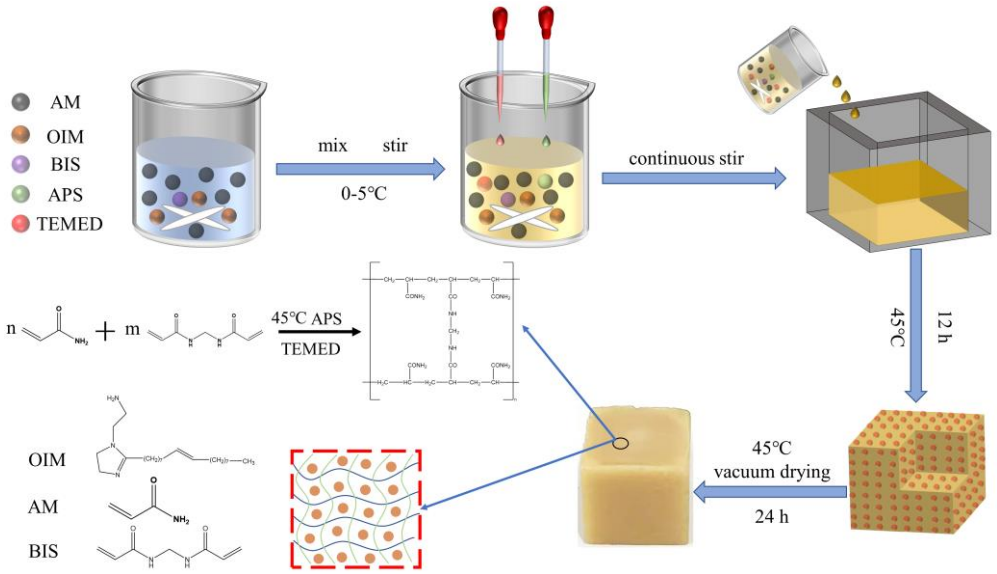

Figure 1. Schematic diagram of the synthesis of OIM@PAM intelligent corrosion inhibitors.

2.2 Characterization methods

The micromorphology of OIM@PAM is observed by Scanning electron microscope (ZEISS EV0 MA15, Carl Zeiss, USA) with the accelerating voltage of 20 KV. The structure of OIM@PAM was measured by Fourier transform infrared analyzer (Nicolet 6700, Thermo Scientific, USA) with wavelength range of 500 cm^{-1}-4000 cm^{-1}. Thermo-gravimetric analysis (DSC823, METTLER TOLEDO, Switzerland) was employed to estimate the loaded amount of OIM at a heating rate of 10 ℃/min among temperature range of 40℃-600℃ in N_2 atmosphere. Tensile test of OIM@PAM mainly referred to the ASTM standard D822 at room temperature in atmosphere, which was measured by electronic universal testing machine (ETM502C, Wance Co. Ltd, China) with the crosshead speed of 5 mm/min [20].Each sample is measured three times to guarantee the accuracy of results. Raman spectrometer (BWS465-785S, B&W TEK, USA) was used to study the OIM adsorption behavior at L80 steel/corrosive solution interface. The selected laser wave length is 785 nm.

2.3 Release behavior of OIM from OIM@PAM

UV-visible spectrophotometer was used to investigate the release behavior of OIM form OIM@PAM. The standard OIM solution with concentration of 50, 100, 125, 150, 175 and 200 mg/L were prepared. The UV-vis curves of standard OIM solution were shown in Figure 2a. And the relationship between absorbance and OIM concentrations was linearly fitted and shown in Figure 2b.

To investigate the OIM release behavior form OIM@PAM, OIM@PAM was completely immersed in 100 ml solution with various pH (3, 5, 7, 9, 11). After a certain time (2 h, 4 h, …), 5 ml immersion solution was taken out and used to test the OIM concentration by UV-vis, and the OIM release amount can be calculated according to OIM standard

Preprints (www.preprints.org) | NOT PEER-REVIEWED | Posted: 27 December 2022 doi:10.20944/preprints202212.0512.v1

curve (Figure2). At the same time, the rest solution was replaced by appropriate pH solution to simulate the flow state of corrosive medium. According to the results of releasing test and TGA test, the cumulative release ratio of OIM from OIM@PAM can be calculated.

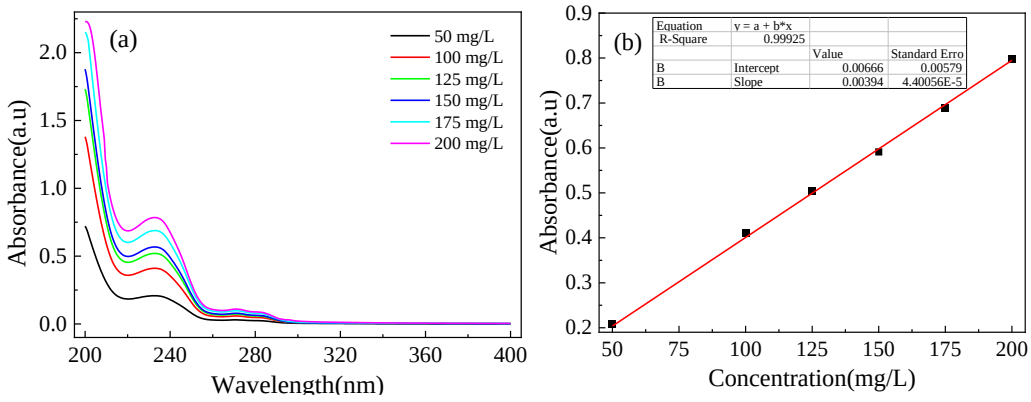

Figure 2. (a): UV-vis spectra for different OIM solutions of known concentration; (b): the fitted standard curve of OIM.

2.4 Corrosion protection performance of OIM@PAM

The L80 carbon steel (wt. %: 0.36%C, 0.45%Si, 1%Mn, 0.03%P, 0.004%S, 0.25%Ni, 0.38%Mo, and balance Fe) purchased from China Jiangsu Xinyou Instrument Co., Ltd was used as corrosion substrate. The surface of L80 coupons were polished by 160# to 2000# SiC grit paper, and rinsed with acetone, deionized water and ethanol. 3.5 wt.% NaCl solutions with different pH values (3, 5, 7, 9, 11) were selected as corrosive medium. The above-mentioned reagents were purchased from Chengdu Kelong Chemical Reagent Factory.

The corrosion protection performance of OIM@PAM on L80 steel in wide range pH values environment was tested by weight loss experiment. The original quality L80 samples were firstly recorded using analytical balance with the precision of ± 0.1 mg. Then L80 samples were immersed in different pH values 3.5 wt.% NaCl solution with and without OIM@PAM. The above experiments were carried out at 25 ℃, and the corrosive solution were regularly replaced every 24 h.

Corrosion products were removed using the acid washing solution composed of 10% HCl + 0.5% ammonioformaldehyde ($C_6H_{12}N_4$)[21]. After that, each L80 sample was weighted three times though electronic balance to ensure the reliability of tested data. The corrosion rate (CR) and inhibition efficiency (IE) of L80 is calculated according to following equations[22].

$$CR = \frac{\Delta w \times 87600}{St\rho} \quad (1)$$

$$IE(\%) = \left(1 - \frac{CR}{CR_0}\right) \times 100 \quad (2)$$

Where Δw with the unit of gram (g) is the mass diffidence of L80 before and after experiment. S with the unit of square centimeter (cm^2) is the surface of L80. t with the unit of hour (h) is the experiment time of L80. ρ with the unit of gram per cubic centimeter ($g \cdot cm^{-3}$) is the density of L80. CR and CR_0 with the unit of millimeter per year ($mm \cdot y^{-1}$) is the corrosion rate of L80 in the medium with and without OIM@PAM respectively.

3. Results and Discussion

3.1. Characteristic of OIM@PAM

3.1.1. Surface morphology of OIM@PAM

Figure 3 shows the surface and interior morphologies of synthesized PAM hydrogel and OIM@PAM. It is clear that OIM loaded into PAM hydrogel causes different morphology. For the PAM hydrogel (Figure 3a and 3b), the surface and interior morphology is relatively smooth and flat without pore canals. This result is due to the surface tension of water and PAM interface, which lead to the tightly bonding between PAM molecules

 doi:10.20944/preprints202212.0512.v1

during the evaporating progress [23]. While the surface and interior morphology of OIM@PAM includes numerous pore canals, which is the characteristic structure of hydrogel container loaded with corrosion inhibitors after vacuum drying [15]. The pore canals existed in OIM@PAM can provide space for OIM accommodation and release.

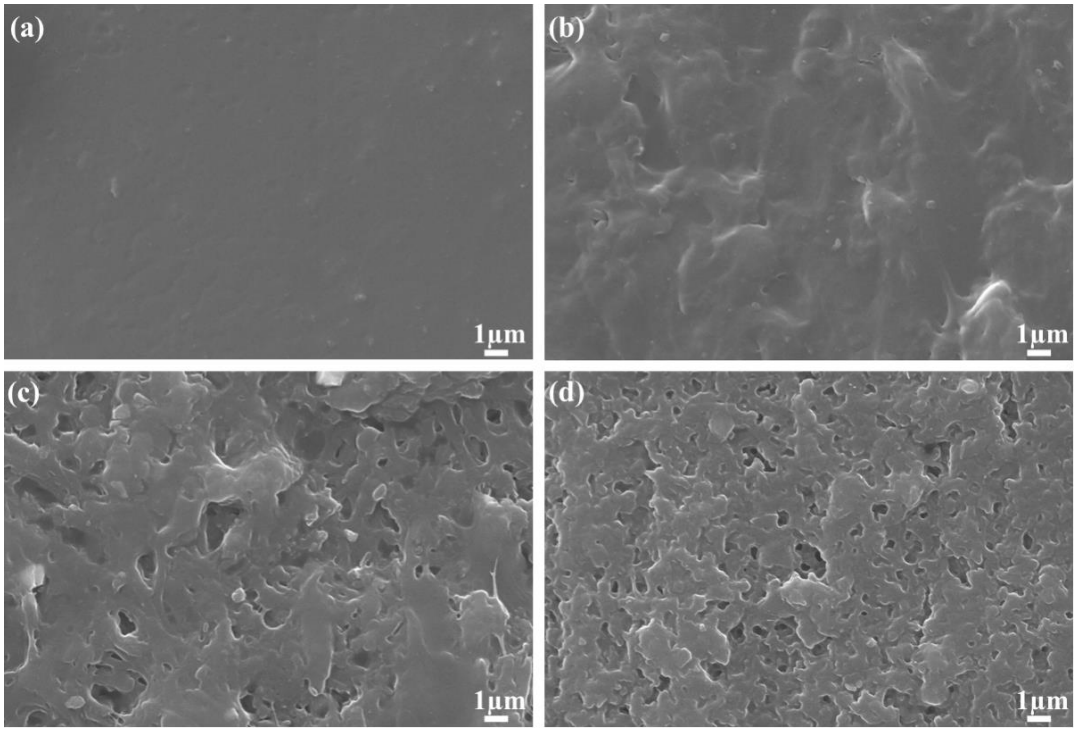

Figure 3. The surface(a) and interior (b) SEM micrographs of the as-prepared PAM after vacuum-dried; The surface(c) and interior (d) SEM micrographs of the as-prepared OIM@PAM after vacuum-dried.

3.1.2. FT-IR analysis

Figure 4 illustrates the FT-IR spectra of OIM@PAM, and the pure OIM and PAM were also tested as control sample. The high-intensity broad absorption peak located in 3440 cm^{-1} is assigned to the antisymmetric stretching vibration of -NH- group existed in OIM, PAM and OIM@PAM [24,25]. The sharpened peak at 1640 cm^{-1} is contributed to the -C=C-, -C=N- and -C=O- double bond [10,25], which can be found in OIM, PAM and OIM@PAM. The stronger peak at 1640 cm^{-1} of OIM@PAM than PAM indicates the load of OIM corrosion inhibitor. There are several characteristic peaks only appears in OIM and OIM@PAM FT-IR spectra. The weak peaks at 2923 cm^{-1} and 2861 cm^{-1} correspond to the symmetric and antisymmetric stretching vibrations of -CH_2- group, respectively. which only consisted in OIM and OIM@PAM [26]. The interferential peak at 2359 cm^{-1} is associated with the antisymmetric stretching vibration of CO_2 due to infrared spectrometer optical path imbalance [27]. And the peak located in 1290 cm^{-1} is attributed to the stretching vibration of tertiary amine group in OIM's imidazole ring [10,24]. Above peaks show a strong indication of OIM was successfully loaded in PAM hydrogel. In addition, there is no new peak in OIM@PAM in compare with the FT-IR spectra of OIM or PAM. The OIM is doped into the network structure of PAM without chemical reaction, which results is consistent with the interior morphology of PAM hydrogel.

Preprints (www.preprints.org) | NOT PEER-REVIEWED | Posted: 27 December 2022 doi:10.20944/preprints202212.0512.v1

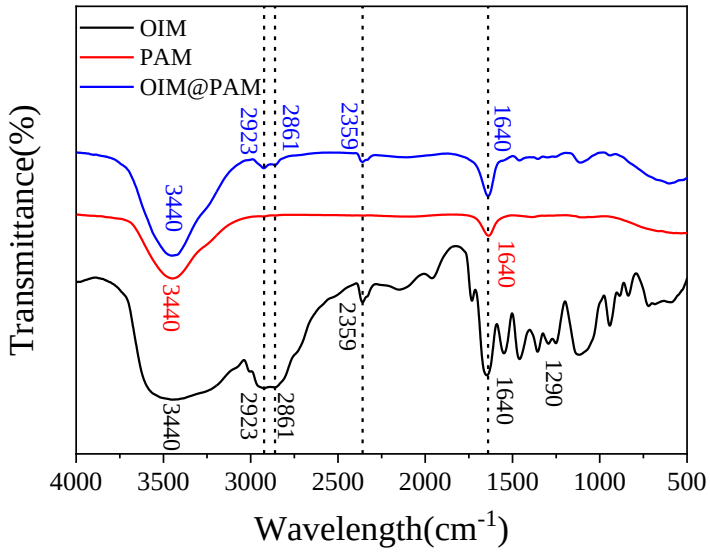

Figure 4. FT-IR spectra of pure OIM, PAM and OIM@PAM

3.1.3. Thermostability and inhibitor loading content of OIM@PAM

Figure 5 compares the thermal gravimetric analysis (TGA) results of OIM, PAM and OIM@PAM. The investigated OIM and PAM hydrogel showed two main degradation stages. The first stage is related to the evaporation of water molecules and other volatile impurities through dehydration [28]. For OIM, the weight loss of this stage (40-190℃) is 8.56%. And for PAM hydrogel, the weight loss of the first stage (40-190℃) is 6.48%. These results reveal the water content in PAM is fewer than that of OIM. More importantly, the OIM have better thermal stability in comparison with PAM. The second stage is related to the decomposition [28,29]. OIM started decomposition at 190℃, and achieved the maximum decomposition rate at 375℃. The mass change of OIM stopped at 500℃, the weight loss is 86.03%, and 3.60% substance remained. The decomposition of PAM starts at about 190℃, and reached the highest decomposition rate at about 400℃. The weight loss of PAM is 66.30%, which is mainly due to the intramolecular and intermolecular imidization reactions on amide group of PAM. This imidization reactions occurred when the temperature reached 190 ℃, and accordingly released NH_3, H_2O and CO_2 [30].

For the TGA curve of OIM@PAM, the first weight loss stage is at 40-190℃. The weight loss caused by water volatilization is about 6.93%. As the temperature increased to 250℃, the TGA curve of OIM@PAM is parallel to that of PAM. This result is due to the high thermal stability of OIM at this temperature, and the weight loss of synthesized composition is mainly cause by PAM. As the temperature further increased, the OIM@PAM rapidly decomposed. OIM@PAM got the highest decomposition rate at about 375℃, which is consisted with OIM. The capacity of OIM in OIM@PAM could be calculated by the decomposition ratio of TGA curves using following equation (3) [31]:

$$D_{OIM} \times C_{OIM} + D_{PAM} \times C_{PAM} = D_{OIM@PAM} \quad (3)$$

Where D_X is the decomposition ratio of compound, and C_X is the content of OIM or PAM in OIM@PAM. Therefore, the content of anti-corrosion inhibitor OIM loaded in the OIM@PAM is 39.64%, which is a quite high value in compare with other researches [32,33]. The TGA results reveals the excellent thermal stability of synthesized OIM@PAM, which could be used in the corrosion environment of temperature lower than 190℃. And the high OIM load content could ensure the anti-corrosion performance of this intelligent inhibitor, which will discuss in follow section.

Preprints (www.preprints.org) | NOT PEER-REVIEWED | Posted: 27 December 2022 doi:10.20944/preprints202212.0512.v1

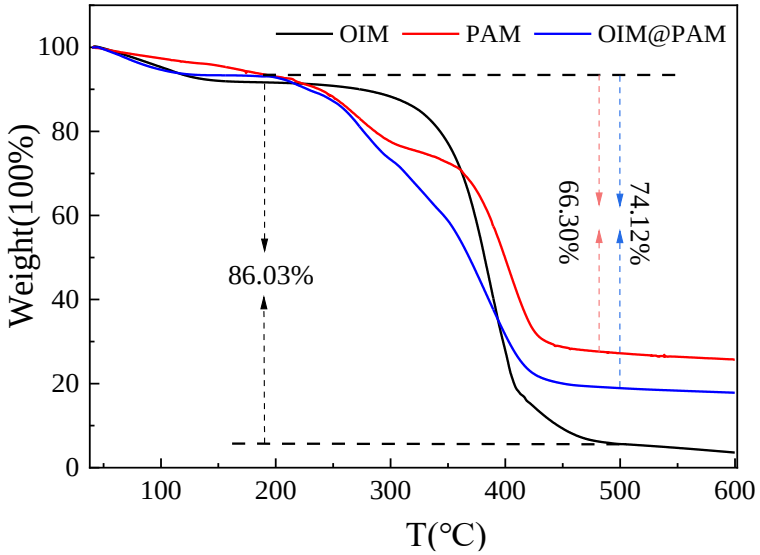

Figure 5. TGA curves of pure OIM, PAM and OIM@PAM

3.1.4. Mechanical properties of OIM@PAM

Appropriate mechanical property is the premise to ensure the practical application of OIM@PAM in corrosion environment, especially for the flowing harsh corrosion environment. The stress-strain curves of PAM hydrogel and synthesized OIM@PAM are shown in Figure6. The average tensile strength (σ_b) value of PAM and OIM@PAM are 17.69 MPa and 13.21 MPa, respectively. Compared with PAM, the hybrid of OIM into PAM leads to the decrease of OIM@PAM strength and the remarkable increase of elongation at break. From TGA analysis, the OIM load content in OIM@PAM is 39.64%, and the PAM content is almost 60.36%. The hybrid of OIM into PAM lead to the monomer concentration of PAM decreasing, and weakening the length of PAM polymer chains. PAM with shorter chain length resulted in the physical entanglement strength decreases and the lower tensile strengths of OIM@PAM [34]. When OIM@PAM sample was stretched, Reversible non-covalent interactions between PAM network and OIM, such as π-π stack and hydrogen bond, etc., can break to effectively dissipate energy and prevent crack propagation, thus increasing its elongation at break [35].

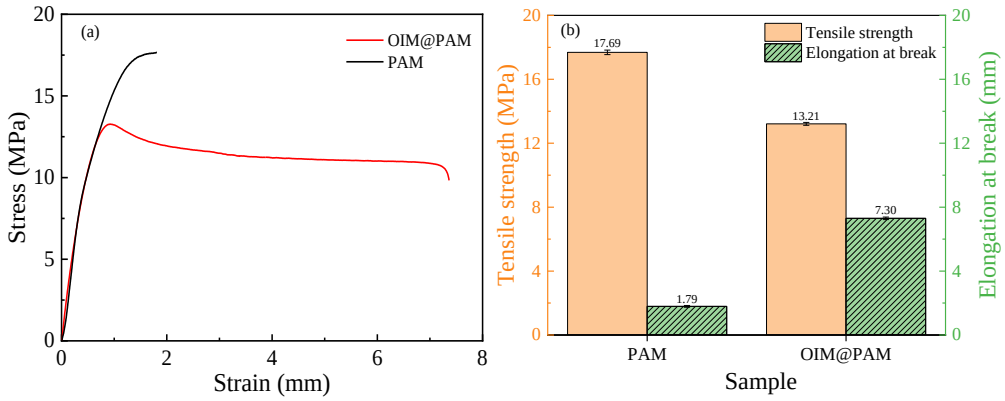

Figure 6. Tensile stress-strain curve of PAM and OIM@PAM after vacuum-dried for 24 h at 45 ℃

3.2. Inhibitor releasing characteristics and mechanism of OIM@PAM

3.2.1 Release behavior of OIM@PAM in different pH environment

Figure 7 shows the release behavior of OIM@PAM in wide range pH solutions. From Figure 7a, the concentration of OIM in test solutions declines as the immersion time increases. In the first 24 h, the inhibitor concentration decreases form over 350 mg/L to about 100 mg/L. As the releasing time further increases, the inhibitor OIM concentration

Preprints (www.preprints.org) | NOT PEER-REVIEWED | Posted: 27 December 2022 doi:10.20944/preprints202212.0512.v1

maintains at several dozen mg/L. The two release stages might be caused by the different releasing mechanism. OIM is a highly effective corrosion inhibitor in various corrosive environment. In our previous study [9], the inhibition efficiency of 10 mg/L OIM in simulated 3.5 wt.% NaCl corrosion environment could reach up to 92%. The inhibitor release behavior of OIM@PAM in different pH solution has no definite difference. The released OIM concentration in pH 3 solution is the highest, which could reach 60 mg/L after 168 h immersion. As the immersion solution pH increased to 7, the released OIM concentration after 168 h decreased to about 20 mg/L. As the solution pH value further increase, the OIM concentration increased to 30 mg/L. Figure 7b shows the cumulative release ratio of inhibitor from OIM@PAM in different pH solutions. In the first 24 hours, the cumulative release ratio of inhibitor reached about 20% to 30% for each condition. As the release time increases, the apparently increasing release ratio could be observed. After 168 h release test, the cumulative release ratio of test sample in pH 3 solution reached the highest value, 81.09%. As the test solution pH value increased, the release ratio decreases obviously to neutral environment, and then slightly increased in alkaline solution. The release behavior of OIM from OIM@PAM is directly affected by pH value of solution.

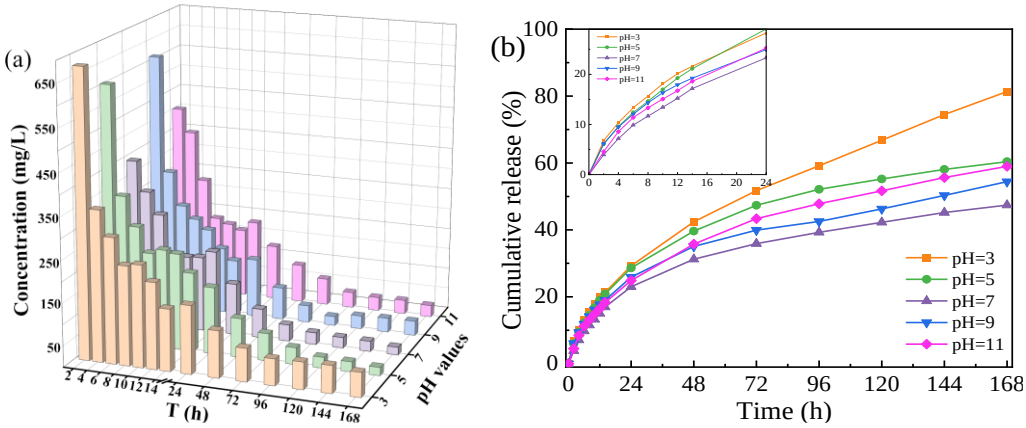

Figure7. the three-times-tested average concentration (a) and the cumulative release (b) of OIM from OIM@PAM in different pH solution at 25 ℃.

3.2.2 Release mechanism of OIM@PAM

From Figure 7, two release stages of OIM@PAM could be observed [36]. When OIM@PAM was immersed in solution, OIM could release quickly through the short diffusion path in the first 2 h, which leads to the high concentration of OIM in the first 2 h. the OIM concentration gradually decreased during 2 to 24 h in the releasing process, which is related to the enlargement of transport path of OIM from the interior of OIM@PAM to test solution. As the immersion time increased, the decrease of OIM amount in OIM@PAM and the increase of transport distance leads to the released OIM concentration continues declining during 24 h to 168 h. The two release stages of the cumulative release curve were fitted by Korsmeyer-Peppas equation [15,37,38] and Parabolic equation [39,40], respectively.

$$\text{Stage I (0 to 24 h): Korsmeyer -Peppas: } \frac{M_t}{M_\infty} = kt^n \quad (4)$$

$$\text{Stage II (24 to 168 h): Parabolic: } \frac{(M_t/M_\infty)}{t} = kt^{-0.5} + a \quad (5)$$

Where M_t and M_∞ are the cumulative release ratio of OIM at time t and infinite time, respectively. k is the release behavior kinetic constant, which is associated to the OIM delivery system. For the Korsmeyer-Peppas model in the first stage, n is an important exponent, which could determine the release mechanism of OIM from OIM@PAM [15] . If $n \leq 0.45$, the release mechanism follows Fick diffusion, and the inhibitor release is controlled by inhibitor concentration gradient [41,42]. If $0.45 < n < 0.89$, the release mechanism is dominated by Anomalous transport or non-Fick transport [15,43]. If $n \geq 0.89$, the release behavior is followed Case II transport [41,43], which means the release rate is only

Preprints (www.preprints.org) | NOT PEER-REVIEWED | Posted: 27 December 2022 doi:10.20944/preprints202212.0512.v1

controlled by the matrix relaxation [41]. For the second stage, a is a constant. The parabolic model of second stage indicates a sustainable release range [40]. All fitted results are presented in Figure 8, and the fitted parameters are presented in Table 1.

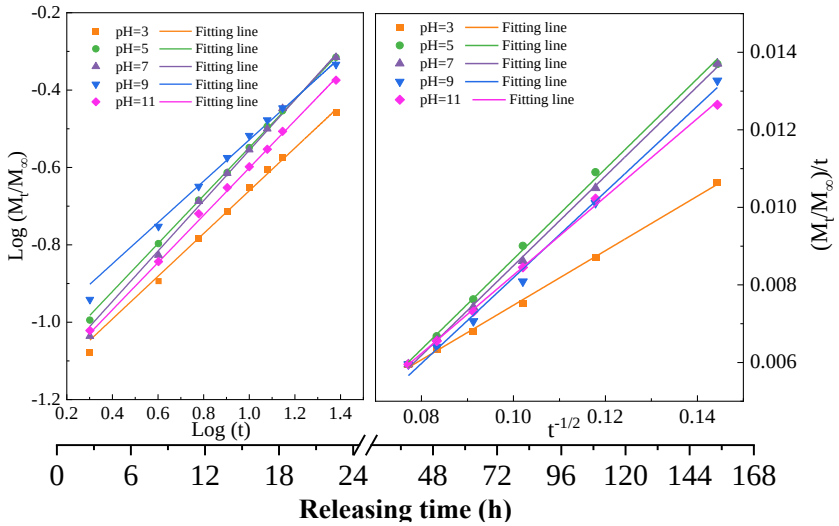

Figure 8. Plots of the two kinetic models: (a) Korsmeyer-Peppas model and (b) Parabolic model for the release of OIM from OIM@PAM in the two stages.

Table 1 the fitting parameter and mechanisms of OIM from OIM@PAM in different pH solutions

pH value	Stage 1 (0~24 h)				Stage 2 (24~168 h)			
	Korsmeyer-Peppas model				Parabolic model			
	n	k	R^2	Release mechanism	k	a	R^2	Release mechanism
3	0.5340	0.00351	0.9952	Anomalous transport	0.07034	0.00044	0.9978	Sustainable release
5	0.7435	0.0028	0.9962	Anomalous transport	0.1304	-0.00413	0.9998	Sustainable release
7	0.6514	0.0033	0.9949	Anomalous transport	0.1156	-0.00307	0.9988	Sustainable release
9	0.5526	0.0612	0.9960	Anomalous transport	0.1106	-0.00288	0.9918	Sustainable release
11	0.6114	0.0033	0.9939	Anomalous transport	0.1010	-0.00185	0.9984	Sustainable release

Figure 9 shows the schematic of the two OIM releasing stages. For the first stage, the OIM release behavior is in good agreement with Korsmeyer-Peppas equation, the fitted R2 is above 0.99. The n values for this stage in different pH solution are in the range of 0.45~0.89, which indicates the inhibitor release mechanism is in accorded with the anomalous transport [15,43]. The inhibitor release behavior is controlled by both diffusion and matrix relaxation [41]. The released OIM due to diffusion mechanism follows Fick's law (Eq. 6).

$$\frac{\partial c}{\partial t} = D\frac{\partial^2 c}{\partial x^2} \qquad (6)$$

Preprints (www.preprints.org) | NOT PEER-REVIEWED | Posted: 27 December 2022 doi:10.20944/preprints202212.0512.v1

The matrix relaxation of PAM gel is due to the absorption of water to the gel 3D network. And the swelling of PAM network caused by water invaded results in the release of inhibitor. The OIM could dissolve in water. Once the OIM in OIM@PAM contact with corrosion medium, the dissolution of OIM became the initial dynamic force of inhibitor releasing. The process of water invaded into gel also follows Fick's second law [44,45], which means the axial water transfer is according to the concentration-dependent diffusivities (Eq. 7).

$$\frac{\partial C_w}{\partial t} = \frac{\partial}{\partial z}\left(D_w \frac{\partial C_W}{\partial z}\right) \qquad (7)$$

Where C_w is the water concentration in hydro-gel, z is the water transfer distance, t presents the time, and D_w is the diffusion coefficient of water in the PAM gel at time t. Since it was assumed that the diffusion coefficient depends on solvent concentration (water in this study), the Fujita model of free volume was used to model solvent ingress kinetics[44,46] (Eq. 8):

$$D_w = D_{w,eq} \exp\left(-\beta_w \left(1 - \frac{C_w}{C_{w,eq}}\right)\right) \qquad (8)$$

Where, $D_{w,eq}$ is the diffusion coefficient of water in the fully swollen PAM, β_w is a structural parameter related to the PAM swelling rate, which will further disused in 3.2.3 section. And $C_{w,eq}$ is the water concentration in the fully swollen PAM. In addition, this model is only concerned with the initial absorb of water, and the water concentration change in PAM at t=0 and x=0 is zero. The absorbed water into PAM gel could replace the inhibitor, so that the inhibitor content released into solution equal to the volume fraction of inhibitor in PAM gel (Eq. 10).

$$C_{inh} = \frac{V_{inh}}{V_{hydro-Gel}} C_w \qquad (9)$$

The total released amount of OIM is consisted of Fick diffusion and hydro-gel swelling, as shown in Eq.10:

$$Q_t = Q_f + Q_s \qquad (10)$$

Where Q_t is the total release amount of inhibitor, Q_f and Q_s is the release amount of inhibitor followed Fick and non-Fick diffusion, respectively. For this stage, the release behavior of OIM@PAM shows little difference in various pH immersion solution. On one hand, the pH value of solution has no influence on the release behavior of Fick diffusion. That is, Q_f of OIM@PAM release behavior has no different in various immersion solution. On the other hand, the different dissolve behavior of PAM in solution with various pH value caused the difference of releasing behavior. And the dissolve behavior of PAM will be discussed later. In brief, in the first stage, the stable status of OIM@PAM leading to the little difference of inhibitor releasing behavior at various pH value.

Preprints (www.preprints.org) | NOT PEER-REVIEWED | Posted: 27 December 2022 doi:10.20944/preprints202212.0512.v1

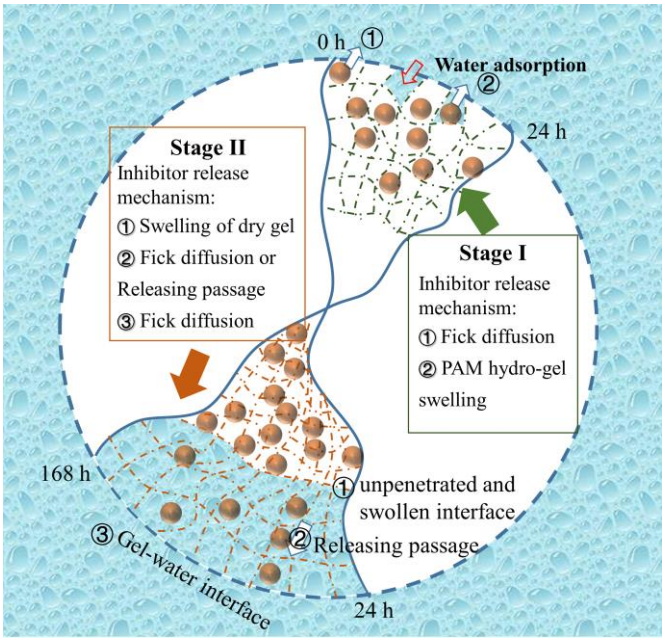

Figure 9. schematic of two releasing stages of inhibitor from OIM@PAM

For the second stage, the inhibitor release behavior turns into Parabolic model. As the releasing time increased, the water penetrated into the PAM hydrogel and leaded to the swelling of the hydrogel. The major effect of water penetrant on the gel entanglement network is the inducement of a viscoelastic stress [47]. During this process, water enhances the mobility of gel chains by converting the glassy matrix into a swollen material. And there are two moving fronts for this process:

(1) a sharp interface between unpenetrated gel and swollen gel (U-S interface), which propagates inwards into the gel.

(2) a gel-water interface (G-W interface), which moves outwards and progressively increases the gel layer thickness.

Several researchers using the water volume fraction Φ(xt) in the gel layer to describe the penetration process and the moving behavior of the two fronts [47–50] :

$$\frac{\partial \Phi}{\partial t} = -\frac{\partial J}{\partial x} = -\frac{\partial}{\partial x}\left(-D\frac{\partial \Phi}{\partial x} + \vartheta_{sw}\Phi\right) = \frac{\partial y}{\partial x}\left(D\frac{\partial \Phi}{\partial x}(1-\Phi)\right) \quad (11)$$

Where D is the water diffusivity in gel material and ϑsw is the swelling velocity of gel. x is the distance between U-S interface and G-W interface.

Assuming the gel material would not dissolve during the immersion process, which means the volume expansion is only caused by water absorption. Therefore, the absorbed water and gel is incompressible and the mixture have no volume change. That is to say:

$$\vartheta_{sw}(x,t) = D\frac{\partial \Phi}{\partial x} \quad (12)$$

For this stage, the OIM release has three steps. Firstly, at the fronts between unpenetrated gel and swollen gel (U-S interface), the swelling of dry gel needs an initiate threshold concentration of water [51]. Therefore, the initial release process of inhibitor at U-S interface is controlled by the initial swelling of gel. And release kinetics of the process could be described by Eq. 8 and 9. Secondly, the diffusion of inhibitor in swollen gel is influenced by viscoelasticity of hydrogel structure [52]. Finally, at the gel-water (G-W) interface, the gel 3D net structure is filled with water. The inhibitor release behavior could be regarded as equilibrium states, which is only followed by Fick's law.

3.2.3 Swelling behavior and micro morphology of OIM@PAM

The macro morphology and volume change of OIM@PAM before and after 168 h releasing test are presented in Figure S1 and Figure 10, respectively. Before the releasing test, the length of cube shape OIM@PAM is 12.5 mm and the surface color is yellow, which

Preprints (www.preprints.org) | NOT PEER-REVIEWED | Posted: 27 December 2022 doi:10.20944/preprints202212.0512.v1

is main due to the color of OIM. After 168 h test, the shape of OIM@PAM is still cube, which indicates the intelligent inhibitor could maintain mechanic strength during the immersion time. The surface color of OIM@PAM has faded, especially for that immersed in pH 3 solution. in combination with the OIM releasing curves in Figure 7, the faded of OIM@PAM is caused by OIM releasing. The side length of inhibitor cube after immersion has grown longer significantly in compare with the pristine cube. These results indicating the swelling rate of OIM@PAM is related to the pH value of corrosive solution. According to Figure 10, the volume change rate of OIM in pH 3 solution is about 85 mm^3/h, which is the highest one of all test condition. And the change rate decreases as the immersion solution pH increases to 7, and then increased as the pH further increase. PAM could have reaction with H+ or OH- in solution [53–55] . In the acid medium, the AM group in PAM would hydrolysis and imidization reactions [53] . As the medium pH decreases, the imidization reaction would be the major reaction. In the alkaline solution, PAM would hydrolysis into acrylic acid and ammonium salt [53,54]. Therefore, the volume change of PAM during immersion is composed by three factors: (1) the swelling of hydro-gel during immersion, (2) the dissolve of PAM material in aqueous environment, (3) the release behavior of inhibitor. It follows from the above that the volume change of gel material is larger than the diffusion flux of water (Eq. 12). This situation could enhance the inhibitor release at the interface between unpenetrated gel and swollen gel. And the initial release step of inhibitor from PAM is strongly affected by the solution pH value.

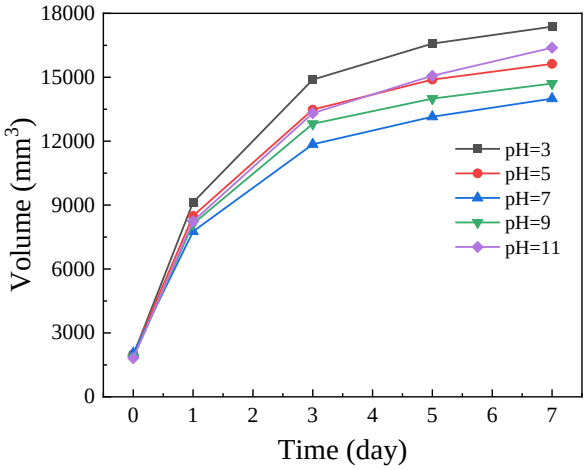

Figure 10. The change in volume of OIM@PAM immersed in various pH test solutions for 7 days.

The internal micro images of the freezing-dried OIM@PAM after 168 h release test in different pH were observed via SEM at 20 KV, and the results are presented in Figure11. For all conditions, the internal morphology showed palisading arrangement due to the evaporation of water during freezing-dried process. The fence-like channel could be the passage of inhibitor releasing. The distribution of channels of intelligent inhibitor in pH 3 and 11 is dense and orderly, and the distance between two channels is about 100 μm. For the inhibitor immersed in pH 5 and 9, the distance between two channels slightly increased. The distribution of channels in PAM inhibitor immersed in pH 7 is much looser than other conditions. This result is consistent with the OIM release results in Figure 7. As we discussed above, the diffusion behavior of inhibitor in swollen gel is controlled by the viscoelasticity of gel structure and Fick's law. Once the swollen gel material forms the ordered channel, the inhibitor release rate will be enhanced. And the distribution of inhibitor pathway could also affect the release behavior.

Preprints (www.preprints.org) | NOT PEER-REVIEWED | Posted: 27 December 2022 doi:10.20944/preprints202212.0512.v1

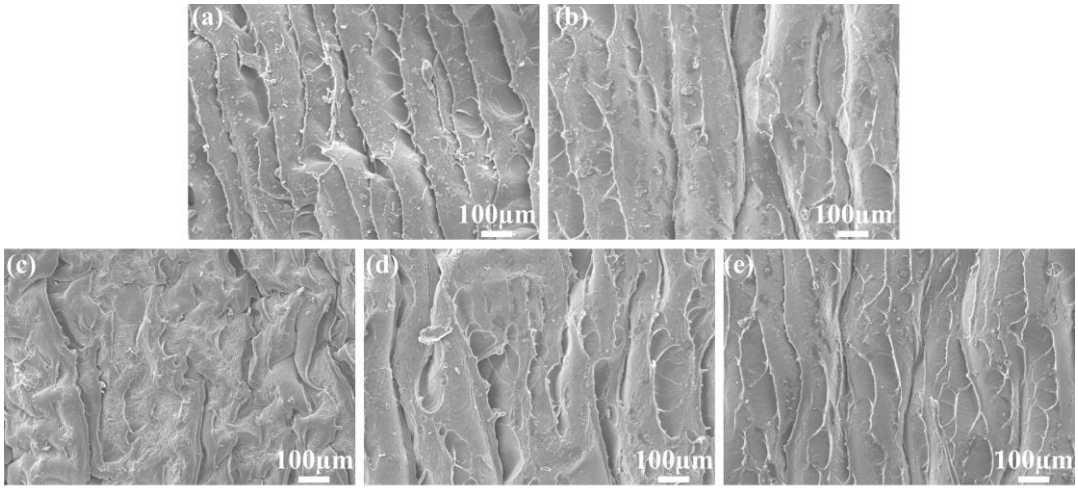

Figure 11. the internal SEM images of OIM@PAM after releasing 168 h in different pH solution. (a) pH 3, (b) pH 5, (c) pH 7, (d) pH 9, (e) pH 11

3.3. Corrosion protection effect of OIM@PAM in various pH NaCl solution

3.3.1 Weight loss measurements

Figure 12 (a) shows the corrosion behavior of L80 steel in the different pH solution of 3.5 wt.% NaCl without OIM@PAM. And the relevant data are listed in Table.S1. The corrosion rate of L80 steel in test solution without intelligent inhibitor is quite high, especially in the acid solution. As the immersion time increase, the corrosion rate of L80 steel in test solutions slightly decreased. After 168 h corrosion test, the corrosion rate of L80 steel remains above 0.2 mm/y, which is severe corrosion for steel in pH 3 and 5, and high corrosion for steel in neutral and alkaline solution according to NACE-RP0775 standard. The unprotected steel in test solution undergoes serious deterioration resulting from electrochemical corrosion. The corrosion mechanism of steel is changed by the pH value of corrosive medium. In acid solution, a localized electrochemical reduction-oxidation reaction is the main corrosion mechanism [56]. For steel immersed in neutral and alkaline NaCl solution, the corrosion rate increases with the pH values augment [57]. The corrosiveness of 3.5 wt.% NaCl solution at different pH for L80 steel long-term soaking follows: pH 3 > pH 5 > pH 11 > pH 9 > pH 7. Therefore, the corrosion protect requirements of L80 steel in various pH value test solution is different, which requires the corrosion inhibitor could adapt the environment and provide appropriate corrosion protection effect.

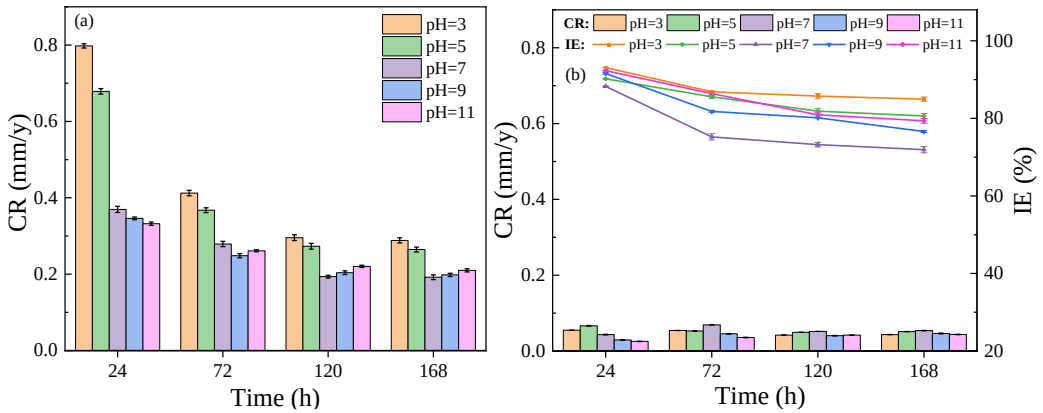

Figure 12. corrosion rate and inhibition efficiency of L80 in different pH solution of 3.5 wt.% NaCl at 25 ℃ with and without OIM@PAM, (a) without OIM@PAM, (b) with OIM@PAM.

Fig 12 (b) shows the corrosion rate of L80 steel in test solutions with OIM@PAM, and inhibition efficiency of inhibitor is calculated. The corrosion rate of L80 steel immersed in inhibited test solutions is dramatically decreased in contrast with in solution without

 doi:10.20944/preprints202212.0512.v1

inhibitor. The released OIM, as a Imidazoline derivatives, could absorb on steel surface and form a hydrophobic film to suppress the corrosion reactions on steel surface [1,9]. N atom in imidazole ring could provide electron to steel surface, which could enhance the adsorption effect of OIM on steel surface. The oleate carbon chain tail in OIM would help to increase the hydrophobicity of the absorption film [58]. The good inhibition performance of OIM is the foundation of the intelligent inhibitor. For the steel immersed in acid solution (pH 3 and 5), the corrosion rate decreased obviously in compare with other condition. After 168 h immersion, the corrosion rate of L80 steel in pH 3 and 5 test solution is 0.0432 mm/y and 0.0511 mm/y, respectively. For the steel immersed in neutral and alkaline solution, the corrosion rate is also reduced to below 0.076 mm/y according to Chinese standards SY/T 5329. The different inhibition effect of OIM@PAM is associated with the corrosivity of test solution and the release characteristics of OIM@PAM. The inhibition efficiency (IE%) calculated by weight loss results are also presented in Figure 14(b) and Table A4. The highest IE% value for each condition was obtained at 24 h, which is due to the quickly release of inhibitor from OIM@PAM in the first release stage (Figure 7). As the immersion time increased, the IE% slightly decreased, especially for the pH 7 solution. This result is due to the release difference of OIM@PAM in various pH solution. According to above discussion, OIM@PAM is an intelligent inhibitor, which could provide appropriate corrosion protection effect for steel in different corrosive medium.

3.3.2 Surface observation of L80 steel after immersion test

Raman spectrum is used to study the adsorption of OIM on L80 steel surface after immersion test, and the results are shown in Figure 13. The pure OIM molecular have three characteristic peaks. The peaks located at 1662 cm^{-1}, 1440 cm^{-1} and 1302 cm^{-1} are attributed to vibration of C=N double bond, C-N bond and -CH_2- group, respectively [9]. For the L80 steel immersed in solution without OIM@PAM, there are characteristic peaks represented of γ-FeOOH (at 250 cm^{-1}, 389 cm^{-1}), α-Fe_2O_3 (at 298 cm^{-1}) and Fe_3O_4 (at 675 cm^{-1}) [59]. For the L80 steel immersed in pH 7 solution with OIM@PAM, the characteristic peaks caused by corrosion products and OIM could both be found. This result indicating the OIM released form OIM@PAM could absorb on steel surface and provide excellent long-term protection performance for steel.

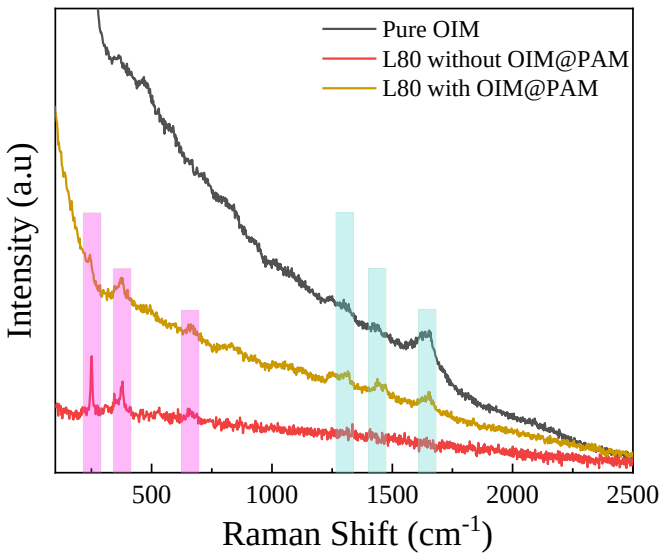

Figure 13. Raman spectrum of pure OIM, L80 immersed in 3.5 wt.%NaCl with and without OIM@PAM after 72 h.

The SEM micrographs of L80 steel after 168 h immersion test in uninhibited and inhibited pH 3, 7 and 11 solutions are presented in Figure 16. According to Figure 14(a), the surface of L80 steel corrode in pH 3 test solution looks similar with the lunar surface. The

 doi:10.20944/preprints202212.0512.v1

rough surface contains several pits with diameter about 30 μm. The surface of steel immersed in pH neutral and alkaline are presented in Figure 13(b) and (c). The corrosion morphology in these conditions shows similar characteristics, which means the corrosion mechanism of these conditions is same. After adding OIM@PAM, the corrosion evidence on steel surface of all conditions shows a significantly reduction. The surface roughness of steel decreases in compare with the uninhibited solution. For the steel in pH 3 inhibited solution, there are some white dots and the polishing traces on steel surface. The surface of steel immersed in pH 7 and 11 inhibited solution shows similar, while the polishing traces on the surface of steel in pH 11 is more obvious than that of steel in pH 7. The SEM results further confirmed the excellent inhibition effect of OIM@PAM in NaCl solution with wide pH range, especially for the more corrosive environment.

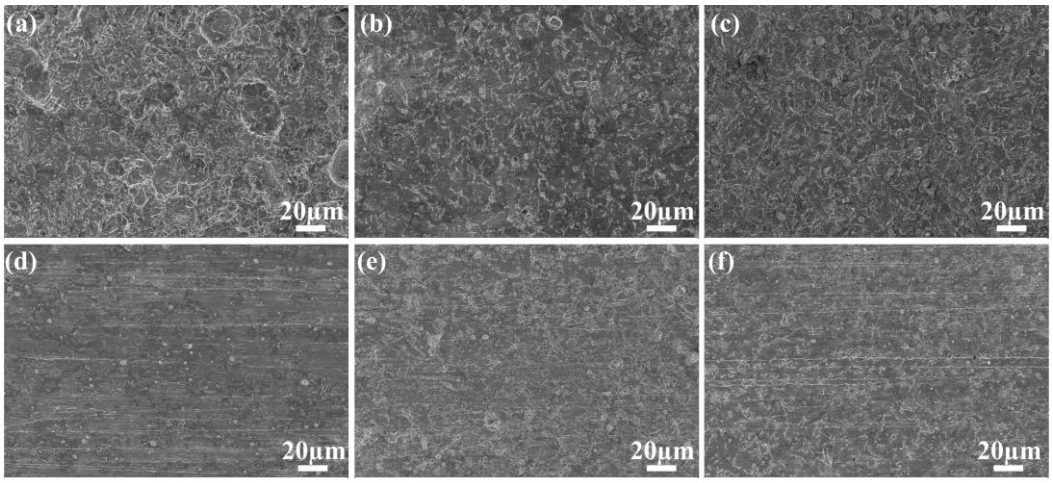

Figure 14. SEM micrographs of L80 steel surface immersed in test solutions for 168 h, (a) pH 3 uninhibited solution, (b) pH 7 uninhibited solution, (c) pH 11 uninhibited solution, (d) pH 3 solution with OIM@PAM, (e) pH 7 solution with OIM@PAM, (f) pH 11 solution with OIM@PAM.

4. Conclusions

(1) OIM is successfully loaded into the PAM gel network, and the load amount is up to 39.64%. The synthesized OIM@PAM have good thermal stability, which could be used in the environment below 190℃. And the OIM@PAM also has good mechanical properties.

(2) The release behavior of OIM from OIM@PAM depends on the external solution pH values, and it release have two stages. The first stage is the OIM quickly release from the PAM, which is followed by Fick' law and hydro-gel swelling. The second stage is the OIM sustained release, which release rate is controlled by the initiate threshold concentration of water for un-swollen gel and inhibitor pathway in the swollen gel.

(3) The intelligent corrosion protection performance of OIM@PAM in wide range pH 3.5 wt.% NaCl solution is checked through weight loss measurement. The corrosion rate of L80 steel in NaCl solution can reduce to below 0.076 mm/y, and the IE% for the OIM@PAM in all conditions are higher than 80%. The Raman and SEM results further confirmed the corrosion protection effect of OIM@PAM.

Supplementary Materials: The following supporting information can be downloaded online, Fig.S1 is the macro morphology of OIM@PAM intelligent inhibitor before and after immersing in different pH solution for168 h. Table A1 is the calculated corrosion rate of L80 and the inhibitor efficiency of OIM@PAM in different pH solutions of 3.5% NaCl with and without OIM@PAM at 25 ℃.

Author Contributions: Qing Yang: Conceptualization, Methodology, Data curation, Writing – original draft. Bing Lin: Methodology, Formal analysis, Data curation, Writing – original draft, Writing – review & editing. Junlei Tang: Conceptualization, Methodology, Resources, Writing – review & editing. Yingying Wang: Writing – review & editing. Hongpeng Zheng: Writing – review & editing. Hailong Zhang: Formal analysis. Zhen Nie: Funding Acquisition. Yanna Zhang: Funding Acquisition.

Funding: This research was supported by the National Natural Science Foundation of China [Grant No. 52201088], Project Funding to the Key R&D Program of Science and Technology Department of Sichuan Province [Grant No. 2021ZYD0099 and 2021ZDZX0002], PetroChina Key technical research on Marine oil and gas development and engineering [Grant No. 2021DJ2503], 2020 Post Doctor Scientific Research Special Foundation of Department of Human Resources and Social Security of Sichuan Province, China.

Data Availability Statement: All raw/processed data necessary for reproducing results in this study can be accessed on reasonable request.

Conflicts of Interest: The authors declare no conflict of interest.

Sample Availability: The synthesized OIM@PAM samples are available from the authors.

References

1. B. Lin, Y. Zuo, Corrosion inhibition of carboxylate inhibitors with different alkylene chain lengths on carbon steel in an alkaline solution, RSC Adv. 9 (2019) 7065–7077. https://doi.org/10.1039/C8RA10083G.
2. I.A.W. Ma, S. Ammar, S.S.A. Kumar, K. Ramesh, S. Ramesh, A concise review on corrosion inhibitors: types, mechanisms and electrochemical evaluation studies, J Coat Technol Res. 19 (2022) 241–268. https://doi.org/10.1007/s11998-021-00547-0.
3. K. Xhanari, M. Finšgar, Organic corrosion inhibitors for aluminum and its alloys in chloride and alkaline solutions: A review, Arabian Journal of Chemistry. 12 (2019) 4646–4663. https://doi.org/10.1016/j.arabjc.2016.08.009.
4. S.A. Haddadi, S.A.A. Ramazani, M. Mahdavian, P. Taheri, J.M.C. Mol, Fabrication and characterization of graphene-based carbon hollow spheres for encapsulation of organic corrosion inhibitors, Chemical Engineering Journal. 352 (2018) 909–922. https://doi.org/10.1016/j.cej.2018.06.063.
5. M. Ormellese, L. Lazzari, S. Goidanich, G. Fumagalli, A. Brenna, A study of organic substances as inhibitors for chloride-induced corrosion in concrete, Corros Sci. 51 (2009) 2959–2968. https://doi.org/10.1016/j.corsci.2009.08.018.
6. F. Seidi, M. Jouyandeh, M. Taghizadeh, A. Taghizadeh, H. Vahabi, S. Habibzadeh, K. Formela, M.R. Saeb, Metal-organic framework (MOF)/epoxy coatings: A review, Materials. 13 (2020). https://doi.org/10.3390/ma13122881.
7. J. Wang, J. Tang, H. Zhang, Y. Wang, H. Wang, B. Lin, J. Hou, H. Zhang, A CO2-responsive anti-corrosion ethyl cellulose coating based on the pH-response mechanism, Corros Sci. 180 (2021). https://doi.org/10.1016/j.corsci.2020.109194.
8. X. Ji, W. Wang, X. Zhao, L. Wang, F. Ma, Y. Wang, J. Duan, B. Hou, Poly(dimethyl siloxane) anti-corrosion coating with wide pH-responsive and self-healing performance based on core−shell nanofiber containers, J Mater Sci Technol. 101 (2022) 128–145. https://doi.org/10.1016/j.jmst.2021.06.014.
9. B. Lin, J. Wang, H. Zhang, Y. Wang, H. Zhang, J. Tang, J. Hou, H. Zhang, M. Sun, Self-healing performance of ethyl-cellulose based supramolecular gel coating highly loaded with different carbon chain length imidazoline inhibitors in NaCl corrosion medium, Corros Sci. 197 (2022). https://doi.org/10.1016/j.corsci.2022.110084.
10. L. Wang, C. Zhang, H. Xie, W. Sun, X. Chen, X. Wang, Z. Yang, G. Liu, Calcium alginate gel capsules loaded with inhibitor for corrosion protection of downhole tube in oilfields, Corros Sci. 90 (2015) 296–304. https://doi.org/10.1016/j.corsci.2014.10.026.
11. P. Ren, D. Zhang, C. Dong, X. Li, Preparation and evaluation of intelligent corrosion inhibitor based on photo-crosslinked pH-sensitive hydrogels, Mater Lett. 160 (2015) 480–483. https://doi.org/10.1016/j.matlet.2015.08.005.
12. Y.N. Wang, C.F. Dong, D.W. Zhang, P.P. Ren, L. Li, X.G. Li, Preparation and characterization of a chitosan-based low-pH-sensitive intelligent corrosion inhibitor, International Journal of Minerals, Metallurgy and Materials. 22 (2015) 998–1004. https://doi.org/10.1007/s12613-015-1161-4.
13. L. Li, C. Dong, L. Liu, J. Li, K. Xiao, D. Zhang, X. Li, Preparation and characterization of pH-controlled-release intelligent corrosion inhibitor, Mater Lett. 116 (2014) 318–321. https://doi.org/10.1016/j.matlet.2013.11.003.
14. J. Liu, S. Qu, Z. Suo, W. Yang, Functional hydrogel coatings, Natl Sci Rev. 8 (2021). https://doi.org/10.1093/nsr/nwaa254.
15. J. Wen, J. Lei, J. Chen, J. Gou, Y. Li, L. Li, An intelligent coating based on pH-sensitive hybrid hydrogel for corrosion protection of mild steel, Chemical Engineering Journal. 392 (2020). https://doi.org/10.1016/j.cej.2019.123742.
16. R.A. Jaal, C. Ismail, B. Ariwahjoedi, A Review of CO2 Corrosion Inhibition by Imidazoline-based Inhibitor, (n.d.). https://doi.org/10.1051/C.
17. Y. Di, X. Li, Z. Chen, X. Yin, Y. Chen, Y. Liu, W. Yang, Experimental and theoretical insights into two fluorine-containing imidazoline Schiff base inhibitors for carbon steels in hydrochloric acid solution, J Mol Struct. 1268 (2022) 133737. https://doi.org/10.1016/j.molstruc.2022.133737.
18. W. Zhuang, X. Wang, W. Zhu, Y. Zhang, D. Sun, R. Zhang, C. Wu, Imidazoline Gemini Surfactants as Corrosion Inhibitors for Carbon Steel X70 in NaCl Solution, ACS Omega. 6 (2021) 5653–5660. https://doi.org/10.1021/acsomega.0c06103.
19. L. Feng, H. Yang, F. Wang, Experimental and theoretical studies for corrosion inhibition of carbon steel by imidazoline derivative in 5% NaCl saturated Ca(OH)2 solution, Electrochim Acta. 58 (2011) 427–436. https://doi.org/10.1016/j.electacta.2011.09.063.
20. X. Cao, B. Zhu, Y. Gao, J. Liu, W. Gao, X. Gai, W. Bao, Process optimization of ultrasound-assisted treatment for soya bean protein isolate/polyacrylamide composite film, R Soc Open Sci. 5 (2018). https://doi.org/10.1098/rsos.180213.
21. Z. Yuan Qiang, Q. Sun, Y. Wang, J. Tang, Y. Wang, H. Wang, Molecular dynamic simulation and experimental investigation on the synergistic mechanism and synergistic effect of oleic acid imidazoline and L-cysteine corrosion inhibitors, Corros Sci. 185 (2021) 109414. https://doi.org/10.1016/j.corsci.2021.109414.
22. J. Shen, D. Yang, L. Ma, Z. Gao, A. Yan, Q. Liao, Exploration of neonicotinoids as novel corrosion inhibitors for copper in a NaCl solution: Experimental and theoretical studies, Colloids Surf A Physicochem Eng Asp. 636 (2022) 128058. https://doi.org/10.1016/J.COLSURFA.2021.128058.
23. J. Hasegawa, K. Kanamori, K. Nakanishi, T. Hanada, S. Yamago, Rigid crosslinked polyacrylamide monoliths with well-defined macropores synthesized by living polymerization, Macromol Rapid Commun. 30 (2009) 986–990. https://doi.org/10.1002/marc.200900066.
24. S. Aayisha, T.S. Renuga Devi, S. Janani, S. Muthu, M. Raja, S. Sevvanthi, DFT, molecular docking and experimental FT-IR, FT-Raman, NMR inquisitions on "4-chloro-N-(4,5-dihydro-1H-imidazol-2-yl)-6-methoxy-2-methylpyrimidin-5-amine": Alpha-2-imidazoline receptor agonist antihypertensive agent, J Mol Struct. 1186 (2019) 468–481. https://doi.org/10.1016/j.molstruc.2019.03.056.
25. Q. Feng, J. Li, H. Cheng, F. Chen, Y. Xie, Hydrogel with lignin for dye, 2014.

26. M.M. Solomon, S.A. Umoren, M.A. Quraishi, D.B. Tripathy, E.J. Abai, Effect of akyl chain length, flow, and temperature on the corrosion inhibition of carbon steel in a simulated acidizing environment by an imidazoline-based inhibitor, J Pet Sci Eng. 187 (2020) 106801. https://doi.org/10.1016/j.petrol.2019.106801.
27. W. Jing-Zun, W. Ting, How to Interpret Infrared (IR) Spectra, University Chemistry. 31 (2016) 90–97. https://doi.org/10.3866/PKU.DXHX201504001.
28. M.S. Hasanin, S.A. al Kiey, Environmentally benign corrosion inhibitors based on cellulose niacin nano-composite for corrosion of copper in sodium chloride solutions, Int J Biol Macromol. 161 (2020) 345–354. https://doi.org/https://doi.org/10.1016/j.ijbiomac.2020.06.040.
29. H. Hassan, A. Salama, A.K. El-ziaty, M. El-Sakhawy, New chitosan/silica/zinc oxide nanocomposite as adsorbent for dye removal, Int J Biol Macromol. 131 (2019) 520–526. https://doi.org/https://doi.org/10.1016/j.ijbiomac.2019.03.087.
30. X. Zhang, M. Han, L. Xu, A.M. AlSofi, Long-term stability prediction of polyacrylamide-type polymers at harsh conditions via thermogravimetric analysis, Chem Phys Lett. 795 (2022) 139538. https://doi.org/10.1016/j.cplett.2022.139538.
31. Y. Huang, T. Liu, L. Ma, J. Wang, D. Zhang, X. Li, Saline-responsive triple-action self-healing coating for intelligent corrosion control, Mater Des. 214 (2022) 110381. https://doi.org/10.1016/j.matdes.2022.110381.
32. P. Ren, D. Zhang, C. Dong, X. Li, Preparation and evaluation of intelligent corrosion inhibitor based on photo-crosslinked pH-sensitive hydrogels, Mater Lett. 160 (2015) 480–483. https://doi.org/https://doi.org/10.1016/j.matlet.2015.08.005.
33. Y. Tian, C. Wen, C. Dong, G. Wang, P. Deng, G. Zhou, An intelligent corrosion inhibitor based on pH sensitive poly(2 diethylaminoethyl methacrylate) microspheres, Int J Electrochem Sci. 14 (2019) 8506–8513. https://doi.org/10.20964/2019.09.04.
34. Z. Li, W. Mi, H. Wang, Y. Su, C. He, Nano-hydroxyapatite/polyacrylamide composite hydrogels with high mechanical strengths and cell adhesion properties, Colloids Surf B Biointerfaces. 123 (2014) 959–964. https://doi.org/10.1016/j.colsurfb.2014.10.050.
35. J. Huang, W. Zhang, H. Li, X. Yu, S. Ding, C. Wu, An autonomous self-healing hydrogel with high polydopamine content for improved tensile strength, J Mater Sci. 55 (2020) 17255–17265. https://doi.org/10.1007/s10853-020-05252-8.
36. X. Li, Y. Di, Z. Chen, W. Yang, pH-responsive bimetallic Ce-ZIF-8 nanocontainer for the active corrosion protection of Al alloys, Colloids Surf A Physicochem Eng Asp. 653 (2022) 129990. https://doi.org/10.1016/J.COLSURFA.2022.129990.
37. X. Xing, J. Wang, W. Hu, Inhibition behavior of Cu-benzoltriazole-calcium alginate gel beads by piercing and solidification, Mater Des. 126 (2017) 322–330. https://doi.org/10.1016/j.matdes.2017.04.024.
38. X. Xing, J. Wang, Q. Li, W. Hu, J. Yuan, A novel acid-responsive HNTs-based corrosion inhibitor for protection of carbon steel, Colloids Surf A Physicochem Eng Asp. 553 (2018) 295–304. https://doi.org/10.1016/j.colsurfa.2018.05.072.
39. E.P. Komarala, S. Doshi, S. Thiyagarajan, M. Aslam, D. Bahadur, Studies on drug release kinetics and antibacterial activity against drug-resistant bacteria of cefotaxime sodium loaded layered double hydroxide-fenugreek nanohybrid, New Journal of Chemistry. 42 (2018) 129–136. https://doi.org/10.1039/c7nj03622a.
40. Y. Wu, Y. Duan, J. Qiu, X. Gao, H. Ma, A pH-responsive intelligent coating based on composite CaCO3 microspheres for long-term corrosion protection of Q235 carbon steel, Appl Surf Sci. 578 (2022) 151980. https://doi.org/10.1016/j.apsusc.2021.151980.
41. M.P. Paarakh, P.A.N.I. Jose, C.M. Setty, G. v Peter, Release Kinetics – Concepts and Applications, International Journal of Pharmacy Research & Technology. 8 (2019) 12–20. https://doi.org/10.31838/ijprt/08.01.02.
42. J. Wen, J. Lei, J. Chen, L. Liu, X. Zhang, L. Li, Polyethylenimine wrapped mesoporous silica loaded benzotriazole with high pH-sensitivity for assembling self-healing anti-corrosive coatings, Mater Chem Phys. 253 (2020) 123425. https://doi.org/10.1016/j.matchemphys.2020.123425.
43. A. Khazaei, S. Saednia, J. Saien, M. Kazem-Rostami, M. Sadeghpour, M.K. Borazjani, F. Abbasi, Grafting amino drugs to poly(styrene-alt-maleic anhydride) as a potential method for drug release, J Braz Chem Soc. 24 (2013) 1109–1115. https://doi.org/10.5935/0103-5053.20130145.
44. G. Thakur, M.A. Naqvi, D. Rousseau, K. Pal, A. Mitra, A. Basak, Gelatin-based emulsion gels for diffusion-controlled release applications, J Biomater Sci Polym Ed. 23 (2012) 645–661. https://doi.org/10.1163/092050611X555830.
45. [45] J. Siepmann, H. Kranz, R. Bodmeier, N.A. Peppas, HPMC-matrices for controlled drug delivery: A new model combining diffusion, swelling, and dissolution mechanisms and predicting the release kinetics, Pharm Res. 16 (1999) 1748–1756. https://doi.org/10.1023/A:1018914301328.
46. H. Fujita, The analytical solution of the fick equation with a concentration-dependent diffusion coefficient in one dimension having infinite vessel limits, J Colloid Sci. 9 (1954) 269–280. https://doi.org/10.1016/0095-8522(54)90022-7.
47. A. Adrover, C. Venditti, M. Giona, Swelling and drug release in polymers through the theory of poisson-kac stochastic processes, Gels. 7 (2021). https://doi.org/10.3390/GELS7010032.
48. J.S. Papanu, D.S. Soane (Soong), A.T. Bell, D.W. Hess, Transport models for swelling and dissolution of thin polymer films, J Appl Polym Sci. 38 (1989) 859–885. https://doi.org/10.1002/APP.1989.070380509.
49. A. Adrover, M. Nobili, Release kinetics from oral thin films: Theory and experiments, Chemical Engineering Research and Design. 98 (2015) 188–201. https://doi.org/10.1016/J.CHERD.2015.04.016.
50. A. Adrover, G. Varani, P. Paolicelli, S. Petralito, L. di Muzio, M.A. Casadei, I. Tho, Experimental and Modeling Study of Drug Release from HPMC-Based Erodible Oral Thin Films., Pharmaceutics. 10 (2018) E222–E222. https://doi.org/10.3390/PHARMACEUTICS10040222.
51. B. Narasimhan, N.A. Peppas, Molecular analysis of drug delivery systems controlled by dissolution of the polymer carrier, J Pharm Sci. 86 (1997) 297–304. https://doi.org/10.1021/JS960372Z.
52. F. Vollmer, J.D. Swaim, M.R. Foreman, Whispering gallery mode sensors, Advances in Optics and Photonics, Vol. 7, Issue 2, Pp. 168-240. 7 (2015) 168–240. https://doi.org/10.1364/AOP.7.000168.
53. V.F. Kurenkov, H.G. Hartan, F.I. Lobanov, Alkaline Hydrolysis of Polyacrylamide, Russian Journal of Applied Chemistry 2001 74:4. 74 (2001) 543–554. https://doi.org/10.1023/A:1012786826774.
54. C.M. Setty, A.S. Deshmukh, A.M. Badiger, Hydrolyzed polyacrylamide grafted maize starch based microbeads: Application in pH responsive drug delivery, Int J Biol Macromol. 70 (2014) 1–9. https://doi.org/10.1016/J.IJBIOMAC.2014.06.027.
55. M.E. Zeynali, A. Rabbii, Alkaline Hydrolysis Of Polyacrylamide And Study On Poly (Acrylamide-Co-Sodium Acrylate) Properties, Iranian Polymer Journal. 11 (2002) 269–275. https://www.sid.ir/en/Journal/ViewPaper.aspx?ID=33881 (accessed September 8, 2022).
56. L. Chen, D. Lu, Y. Zhang, Organic Compounds as Corrosion Inhibitors for Carbon Steel in HCl Solution: A Comprehensive Review, Materials. 15 (2022) 2023. https://doi.org/10.3390/ma15062023.
57. R. Aslam, G. Serdaroglu, S. Zehra, D. Kumar Verma, J. Aslam, L. Guo, C. Verma, E.E. Ebenso, M.A. Quraishi, Corrosion inhibition of steel using different families of organic compounds: Past and present progress, J Mol Liq. 348 (2022). https://doi.org/10.1016/j.molliq.2021.118373.

 doi:10.20944/preprints202212.0512.v1

58. A.S. Fazayel, M. Khorasani, A.A. Sarabi, The effect of functionalized polycarboxylate structures as corrosion inhibitors in a simulated concrete pore solution, Appl Surf Sci. 441 (2018) 895–913. https://doi.org/10.1016/J.APSUSC.2018.02.012.
59. X. Zhang, K. Xiao, C. Dong, J. Wu, X. Li, Y. Huang, In situ Raman spectroscopy study of corrosion products on the surface of carbon steel in solution containing Cl- and SO42-, Eng Fail Anal. 18 (2011) 1981–1989. https://doi.org/10.1016/j.engfailanal.2011.03.007.